Short communication

Co-electrolysis of steam and CO_2 in a solid oxide electrolysis cell with $La_{0.75}Sr_{0.25}Cr_{0.5}Mn_{0.5}O_{3-\delta}$ −Cu ceramic composite electrode

Ruimin Xing [a], Yarong Wang [b], Yongqiang Zhu [a], Shanhu Liu [a, *], Chao Jin [b, *]

[a] Institute of Environmental and Analytical Sciences, College of Chemistry and Chemical Engineering, Henan University, Kaifeng 475004, PR China
[b] College of Physics, Optoelectronics and Energy & Collaborative Innovation Center of Suzhou Nano Science and Technology, Soochow University, Suzhou 215006, PR China

HIGHLIGHTS

- Cu-impregnated LSCM cathode has been prepared and evaluated for co-electrolysis of steam and CO_2.
- Encouraging co-electrolysis performances have been achieved.
- The Cu-impregnated LSCM cathode based SOEC has endured a durability test of over 50 h for co-electrolysis at 750 °C.

ARTICLE INFO

ABSTRACT

Cu impregnation has been performed to improve electronic conductivity of $La_{0.75}Sr_{0.25}Cr_{0.5}Mn_{0.5}O_{3-\delta}$ (LSCM) material in reducing atmosphere, and solid oxide electrolysis cells (SOECs) with the configuration of LSCF|LSGM|LSCM−Cu are prepared and evaluated for high temperature steam and carbon dioxide co-electrolysis. Electrochemical impedance spectra (EIS) and voltage−current curves are carried out to characterize the cell performances. Compared with LSCF|LSGM|LSCM cell without Cu impregnation for steam electrolysis under the same conditions, EIS results show that LSCF|LSGM|LSCM−Cu cell not only displays lower ohmic resistance and better electrochemical performances, but also their resistance increases with the percentage of the fed CO_2 under open circuit voltage, in which the polarization resistance dominates. With the applied electrolysis voltage of 1.65 V and the operating temperature of 750 °C, the maximum consumed current density increases from 1.31 A cm^{-2} without CO_2 to 1.82 A cm^{-2} with 37.5% CO_2. Although there is an increase of 2.0% in the applied electrolysis voltage, the cell has exhibited an excellent durability test for more than 50 h with the electrolysis current density of 0.33 A cm^{-2} and the gas mixture of 50% AH−25% H_2−25% CO_2 at 750 °C.

© 2014 Elsevier B.V. All rights reserved.

1. Introduction

The growing interest of the scientific community towards the global warming and its consequences over environment lead to investigate new energy resources in order to decrease CO_2 emissions and the dependence on fossil fuels. Attractive in its simplicity and high efficiency, high temperature H_2O-CO_2 co-electrolysis in solid oxide electrolyzer cells (SOECs) offers an alternative way to not only convert CO_2 and H_2O to the fuel, but also to store the discontinuous and high transmitting cost electricity to chemical energy [1–3]. Nuclear power and renewable electrical energy can be used to electrochemically convert CO_2 and H_2O to synthesis gas

($CO + H_2$), which would be further used as a feed stock for production of hydrocarbon fuel via the Fischer−Tropsch (F−T) process. At the same time, pure oxygen is obtained as by-products.

More specifically, in the process of co-electrolyzing H_2O-CO_2 to $CO + H_2$ in an SOEC, oxygen ions are detached from H_2O and CO_2 at the cathode and transported to the anode to generate O_2 molecules [4,5]. This can be conducted by conventional solid oxide fuel cells (SOFCs) containing an oxygen-ion-conducting solid oxide electrolyte such as yttria-doped zirconia (YSZ). The feasibility of H_2O-CO_2 co-electrolysis in Ni/YSZ-electrode-supported SOECs was demonstrated by conducting the electrolysis for 500 h at 1123 K [4]. However, the Ni/YSZ electrode was often poisoned by impurities in CO_2 gas, such as S, even though which could be reactivated by introducing hydrogen. Moreover, in the process of co-electrolysis, there might be carbon deposition on nickel from the generated CO [6,7]. More worse, the agglomeration and particle coarsening of

* Corresponding authors.
  E-mail addresses: shanhuliu@henu.edu.cn (S. Liu), jinchao@suda.edu.cn (C. Jin).

metallic Ni in Ni/YSZ based SOECs often happened under SOEC operating conditions, which would lead to a drop in the length of three phase boundary (TPB) where the electrochemical reaction took place [8,9]. Instead of a Ni/YSZ electrode, oxide composite electrodes based on $La_{0.8}Sr_{0.2}Cr_{0.5}Mn_{0.5}O_3$ (LSCM) have also been utilized to electrolyze dry CO_2, demonstrating that dry CO_2 electrolysis could be performed without the addition of a reducing gas such as CO or H_2 [10–13]. LSCM is a p-type conductor with the conductivity of 38 S cm^{-1} at the oxygen partial pressure above 10^{-10} atm. However, the electrical conductivity of LSCM is much lower in the reducing atmosphere (1.5 S cm^{-1} in 5% H_2) [14,15]. The substitution of Sr into the A-site of the LSCM perovskite results in a charge-compensating transition of Cr^{3+}/Mn^{3+} to Cr^{4+}/Mn^{4+}, and the compensation is achieved by the formation of oxygen vacancies at low oxygen partial pressure. Therefore, the ionic conductivity of LSCM increases while the electrical conductivity significantly decreases under the reducing environment. Addition of an electrically conducting phase such as Cu would dramatically enhance the electrical conductivity of the electrode. Thus, CuO is usually incorporated into the porous LSCM matrix by the impregnation method due to its low melting temperature which could be reduced to Cu in the fuel gas during the cell operation [14,16].

In this study, we fabricated a Cu-impregnated LSCM ceramic cathode based SOECs to promote the $H_2O–CO_2$ co-electrolysis performance. In addition, effects of different steam and CO_2 contents were also investigated.

2. Experimental

2.1. Preparation and characterization of LSCM and LSGM materials

$La_{0.75}Sr_{0.25}Cr_{0.5}Mn_{0.5}O_3$ (LSCM) material was prepared through a citric acid–nitrate process as our previous report [10]. Stoichiometric amounts of analytical grade lanthanum nitrate (La(NO$_3$)$_3$·6H$_2$O, Guoyao reagent, 99.9%), strontium nitrate (Sr(NO$_3$)$_2$, Guoyao reagent, 99.0%), chromium nitrate (Cr(NO$_3$)$_3$·9H$_2$O, Guoyao reagent, 98.5%) and 50 wt.% manganese nitrate solution (Mn(NO$_3$)$_2$·4H$_2$O, Guoyao reagent) were dissolved in deionized water with constant stirring at room temperature, and the concentration of total metal ions was 0.2 mol L^{-1}. Citric acid was then added to the mixture as chelating and complexing agent, and the mole ratio of the total metal ions to citric acid was controlled around 1:1.5. Ammonium hydroxide (Guoyao reagent, NH$_3$ content 28.0–30.0%) was added to adjust the pH value to about 6.0. A gel was obtained after the solution was agitated at 80 °C on a hot–plate for 24 h, which was then held at 400 °C for 5 h in an oven to remove organics and form a precursor powder. The $La_{0.75}Sr_{0.25}Cr_{0.5}Mn_{0.5}O_3$ precursor powder was pulverized and then calcined at 1100 °C for 5 h $La_{0.8}Sr_{0.2}Ga_{0.83}Mg_{0.17}O_{3-\delta}$ (LSGM) electrolyte material was prepared by a solid state reaction method as described previously [13,17].

The crystal structure of the powders was examined with X–ray diffraction (XRD) using a Bede D1 X–ray diffractometer (UK, Bede Scientific Ltd.; Cu K$_\alpha$ radiation; operated at 40 kV, 45 mA; $\lambda = 0.15418$ nm), the diffraction angle ranged from 20° to 80° with a step of 0.02° and a rate of 1.2° min^{-1}. A scanning electronmicroscopy (SEM) (FEI Quanta 200) operating at 30 kV was used to characterize the microstructure of single cells.

2.2. Fabrication and measurement of single SOEC

LSGM electrolyte substrates (15 mm in diameter, 0.5 mm in thickness) were formed by pressing LSGM powders uniaxially under 200 MPa, followed by sintering at 1450 °C in air for 10 h. The cathode ink consisting of LSCM powders and V-006 organic binder

(weight ratio of 1:1) was applied to the surface of the sintered LSGM electrolyte by screen-printing method, and then fired at 1150 °C in air for 2 h. The porous anode was prepared using a mixture of $La_{0.6}Sr_{0.4}Co_{0.8}Fe_{0.2}O_3$ (LSCF, Fuel Cell Materials, USA) and LSGM in a weight ratio of 1:1 with an ethyl cellulose–terpineol vehicle. The mixture was screen–printed on the other surface of LSGM electrolyte substrate, followed by a pure LSCF layer, and fired at 1000 °C for 2 h in air. The effective anode area is 0.33 cm^2.

Cu was loaded into the porous LSCM cathode by a wet impregnation method. A drop of aqueous $Cu(NO_3)_2 \cdot 2.5H_2O$ solution (1 M) was placed on LSCM cathode. The surface of the electrode was then wiped with a soft tissue and dried at 175 °C on the hot plate for 20 min. The cathode was calcined at 850 °C for 0.5 h to decompose $Cu(NO_3)_2$ to form CuO. The loading level of CuO can be increased by repeating the impregnation process.

Pt ink was brushed on both LSCM cathode and LSCF anode surface, respectively, and then fired at 1000 °C for 1 h to act as current collector. The catalytic contribution from this Pt ink was considered insignificant, because the type is only used for current collection rather than as electrocatalyst. Pt wires were used to connect the electrodes to electrochemical testing equipment. The fabricated button cells were sealed to one end of an alumina tube with a ceramic paste (Aremco–552 high temperature ceramic adhesive paste). The ceramic paste was cured during the heating up of the cell electrochemical testing to form a gas tight sealing.

The high temperature electrolysis cell testing system is assembled according to the schematic diagram shown in Fig. 1. Here, hydrogen acted as carrier gas and reducing gas to maintain the reducing environment in the cathode with the flow of 30 ml min^{-1}. H_2 and CO_2 contents were controlled through precision mass flow controllers (APEX, Alicat Scientific, U.S.), followed by being mixed with water vapor in a heated humidifier. The absolute humidity (AH, the vol.% of humidity in the total gas volume) was detected using an on-line humidity sensor (Vaisala Model HMP 337) to represent steam concentrations in the electrolysis process. Electrochemical performance of the SOEC cells was studied using a conventional four–electrode method through a CHI6500. Electrochemical impedance spectra (EIS) under OCV with different steam and CO_2 contents were recorded through an IM6e Electrochemical Workstation (ZAHNER, Germany) with the AC amplitude of 10 mV over the frequency range of 100 kHz to 0.1 Hz.

3. Results and discussion

3.1. XRD and SEM characterizations

Fig. 2(a) shows X–ray diffraction patterns of the final LSCM powders after being calcinated in air at 1100 °C for 5 h, indicating the formation of a single perovskite phase. While, Fig. 2(b) is the XRD pattern for the Cu-impregnated LSCM powders after being reduced by hydrogen at 850 °C for 1 h. Compared with the XRD pattern of pure perovskite phase of LSCM powders shown in Fig. 2(a), there is no second phase or peak splitting for the perovskite structure shown in Fig. 2(b), but the Cu characterized peaks at 43.5, 50.6, 74.2° appeared, suggesting that LSCM is chemically compatible with Cu under SOECs working conditions.

In the process of Cu-impregnation, the Cu content plays an important role on the microstructures of the fabricated cathode. If too little Cu, there could not form good interconnection between LSCM and Cu particles; conversely, if too much Cu, the LSCM layers will be completely filled by the Cu particles with lower porosity. Therefore, the optimized 20 wt.% Cu has been directly impregnated in this study according to Zhu's work [16]. Fig. 3(a) presents SEM micrograph of cross–sections of the fabricated SOEC before electrochemical performances test. It can be seen that the cell has a
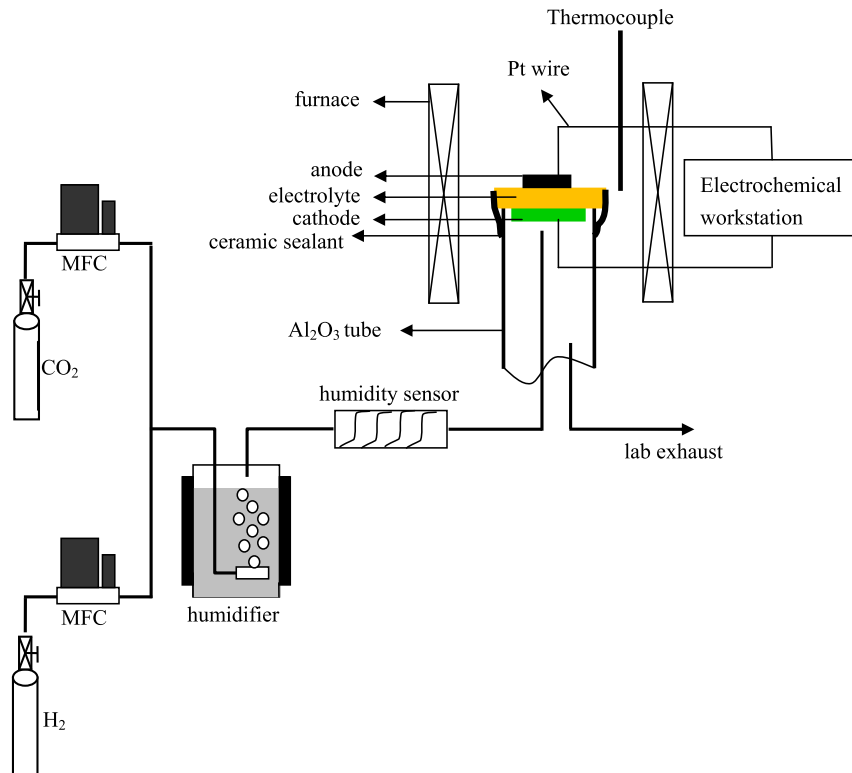
Fig. 1. Schematic of experimental setup for high temperature steam and carbon dioxide co-electrolysis measurements.
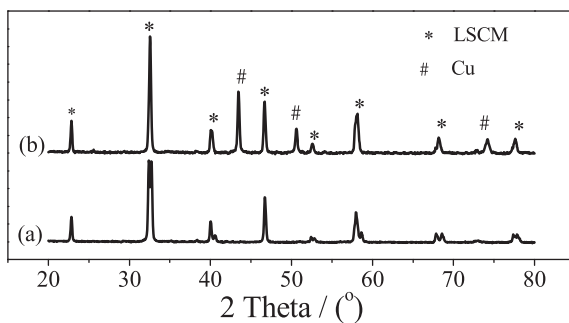
Fig. 2. X–ray diffraction patterns of LSCM powder (a); Cu-impregnated LSCM powder after reduced by H_2 at 850 °C for 1 h (b).

~250 μm dense LSGM electrolyte substrate, ~100 μm porous LSCM–Cu cathode and LSCF anode adhering very well to the LSGM substrate. Fig. 3(b) shows an enlarged image of Cu-impregnated LSCM cathode. After Cu impregnation, the composite cathode was composed of a large LSCM backbone surrounded by submicron-sized Cu particles. A well interconnection was observed between LSCM and Cu particles, which would favor electron transmission. Also, the composite cathode is porous, which could provide enough effective diffusion of reaction gas.

3.2. Electrochemical performances of LSCM|LSGM|LSCF cell

For comparison, a LSCM|LSGM|LSCF cell without Cu impregnation has also been fabricated with the same procedure and tested with 50% AH-50% H_2 as fuel under SOFC and SOEC mode, respectively. Fig. 4(a) shows the typical voltage versus current density
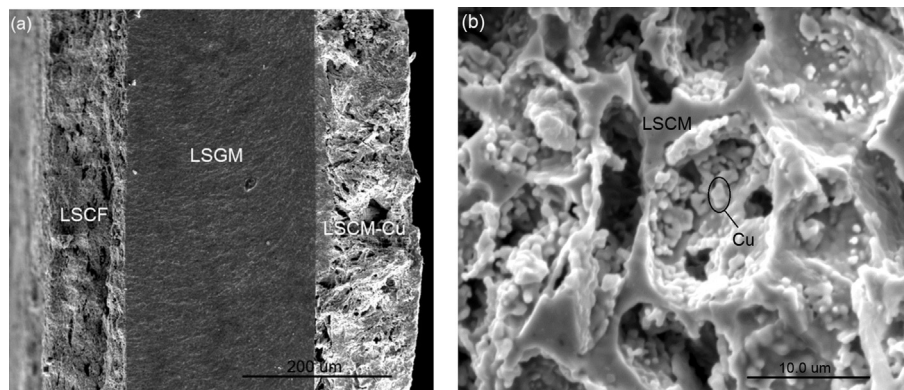
Fig. 3. Crosses-section SEM images of LSCF|LSGM|LSCM-Cu cell before electrochemical test (a); enlarged SEM image of LSCM-Cu cathode (b).
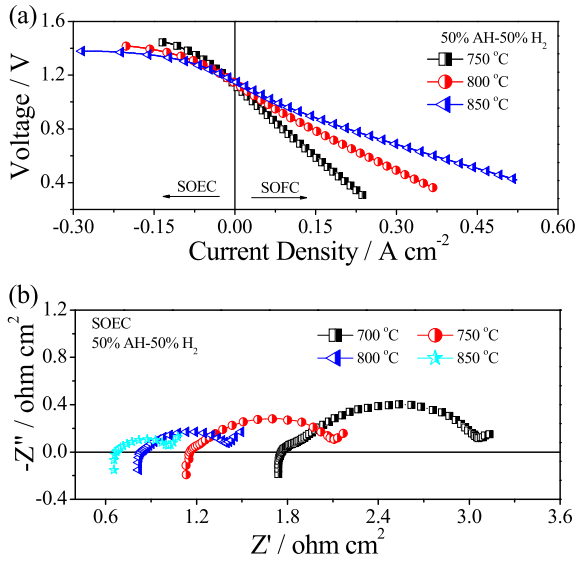
Fig. 4. Voltages–current density curves and impedance spectra of the LSCF|LSGM|LSCM cell with 50% AH–50% H$_2$ at different operated temperatures.

Fig. 5. Voltages–current density curves and impedance spectra of the LSCF|LSGM|LSCM-Cu cell with different steam and carbon dioxide contents at 750 °C.

dependence (*V*–*I* curves) in both SOFC and SOEC modes with 50% AH-50% H$_2$ as fuel with different cell operating temperature of 700, 750, 800 and 850 °C, respectively. The data were collected by scanning potential-current from 1.6 to 0.2 V with 20 mV s^{-1} increments. The negative current densities indicate the power consumption (the SOEC mode) while the positive current densities indicate the power generation (the SOFC mode). The cell voltage at zero current density corresponds to the open-circuit voltage (OCV). From the *V*–*I* curves, it can be observed that there is a smooth transition across the open-circuit voltage from SOEC mode to SOFC mode, which indicates that the LSCM|LSGM|LSCF cell is reversible for the charge transfer reaction. The consumed current density at a given applied electrolysis voltage generally increases with increasing the operating temperature. Fig. 4(b) displays the electrochemical impedance spectra (EIS) of the LSCM|LSGM|LSCF cells measured under open circuit condition with 50% AH-50% H$_2$ as fuel at different operating temperatures. The intercept of the impedance spectra with the real axis at high frequency corresponds to the ohmic resistance (R_s) of the cell, which mainly comes from the YSZ electrolyte and the Pt lead wires. The overall size of the impedance arcs is attributed to the cell polarization resistance (R_p). The intercept of the impedance spectra with the real axis at low frequency corresponds to the total cell resistance (R_t), including the cell ohmic resistance and polarization resistance. The R_s values are 1.7, 1.1, 0.85 and 0.65 Ω cm^2 about at 700, 750, 800 and 850 °C, respectively. Moreover, R_t and R_p also decreased with increasing the operating temperatures.

3.3. Electrochemical performances of LSCM-Cu|LSGM|LSCF cells

Fig. 5(a) shows the typical voltage versus current density dependence (*V*–*I* curves) in both SOFC and SOEC modes with different fuels at 750 °C, respectively. Open circuit voltages were very close to the theoretical Nernst potentials, indicating the presence of a hermetic seal. All *V*–*I* curves evolve smoothly from SOFC to SOEC mode in a linear manner within the sweep range. As shown in Fig. 5(a), OCVs decrease from 1.053 V to 0.847 V with the CO$_2$ to hydrogen ratio increasing. In the hydrogen–steam–carbon dioxide system, the OCVs can be calculated several ways, depending on the half-reaction. There are three possible half–reactions for the hydrogen–steam–carbon dioxide system, as following:
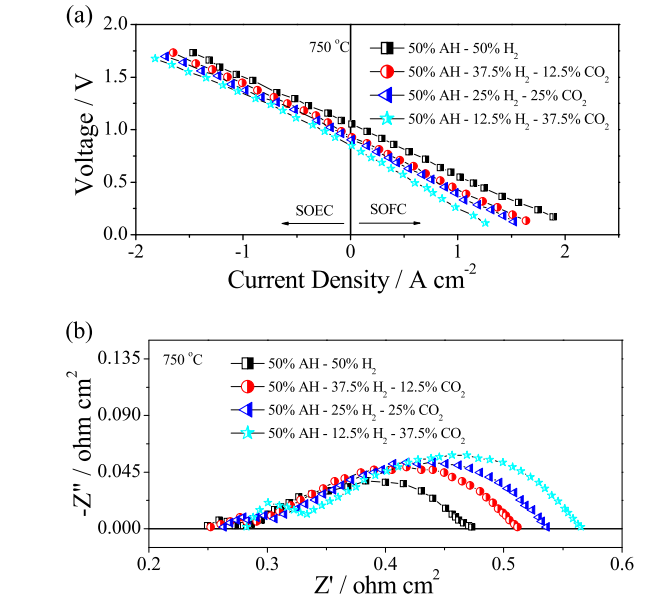
$$H_2O_{(g)} + 2e^- \leftrightarrow H_2 + O^{2-} \tag{1}$$

$$CO_2 + 2e^- \leftrightarrow CO + O^{2-} \tag{2}$$

$$CO_2 + 2H_2O_{(g)} + 6e^- \leftrightarrow CO + 2H_2 + 3O^{2-} \tag{3}$$
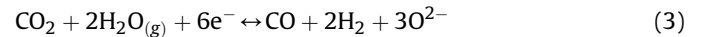
It is difficult to determine which half-reaction is dominant. Assuming that there is only the half-reaction (1), the OCV is controlled by the hydrogen to steam ratio. However, the variations of measured OCVs are bigger than that of calculated OCVs, which is predicted from the Nernst equation [18]. So, we believe it is not a simple reaction mechanism. The half-reaction (2) or (3), even water gas shift reaction maybe be involved. More works need to be done to prove the reaction mechanism with the help of outlet gases analysis.

In the SOEC mode, the voltage varies linearly with the cell current density. It can be seen that reducing the ratio of hydrogen to CO$_2$ could lead to the improvement of the cell current density. For example, according to Fig. 5(a), when the CO$_2$ content was increased from 0 to 37.5 % at 750 °C, the cell current density showed a significant improvement, from 1.31 to 1.82 A cm^{-2} at applied voltage of 1.65 V, comparable to our previous study about steam electrolysis [10]. The current–voltage dependence was generally linear with open circuit but showed a decreasing slope at
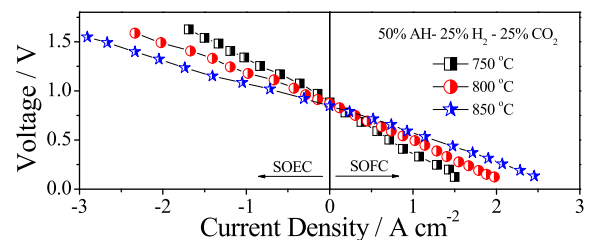
Fig. 6. Voltages–current density curves of LSCF|LSGM|LSCM-Cu cell with 50% AH–25% H$_2$–25% CO$_2$ at different operating temperatures.
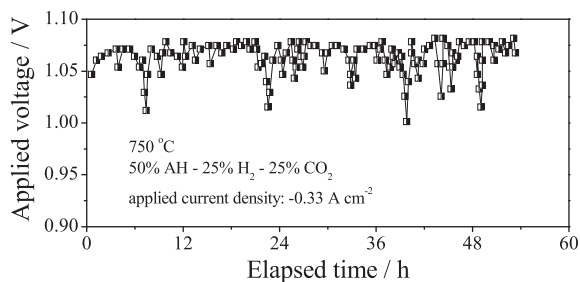
Fig. 7. Short−term durability test of LSCF|LSGM|LSCM-Cu cell with 50% AH−25% H_2−25% CO_2 and 0.33 A cm^{-2} electrolysis current at 750 °C.

sufficiently large applied voltage, suggesting electrode activation polarization.

The electrochemical impedance spectra of the cell, as shown in Fig. 5(b), were also measured under OCV conditions with different fuels at 750 °C, respectively. It can be clearly observed that R_s, R_p and R_t increased with increasing the percentage of the fed CO_2, and the change of R_p is dominant. Based on the thermodynamics of CO_2 and H_2O reduction reactions, the free energy of CO_2 splitting becomes equal to that of H_2O splitting at about 1100 K; therefore, CO_2 and H_2O splitting are almost equally favorable at the operating temperature, i.e., 1023 K [19]. However, according to Barnett's study about CO_2/H_2O co-electrolysis [18], the diffusivities of reactants gas generally decreased with increasing the CO_2 content due to the higher molecular weight of CO_2 compared to H_2O. Furthermore, the R_s value is 0.25 Ω cm^2 with 50% AH-50% H_2 as fuel, which is much lower than that of LSCM|LSGM|LSCF cell at the same conditions, indicating that Cu impregnation effectively improved the electrical conductivity of LSCM.

Fig. 6 shows $V−I$ curves at different operating temperatures with a gas mixture of 50% AH−25% H_2−25% CO_2. Open circuit voltages ranged from 0.87 to 0.90 V and were consistent with the values predicted using the Nernst equation (0.89−0.92 V) [20]. Current density values at a given applied voltage generally increased with increasing the operating temperature, as typically observed for SOECs. The electrolysis current densities increased from 1.5 to 2.9 A cm^{-2} at 1.5 V with increasing the temperature from 750 to 850 °C.

3.4. Cell durability study

Yang and Irvine have done some exploring works to investigate the possibility of LSCM as cathode material in SOECs for steam electrolysis and CO_2/H_2O co-electrolysis; but, they used very low steam concentration (3 vol.% H_2O) and the cell durability test was not demonstrated [21]. Fig. 7 shows the short−term durability performance of the cell operated under a constant electrolysis current density of 0.33 A cm^{-2} with a gas mixture of 50% AH−25% H_2−25% CO_2 at 750 °C. The cell shows a relatively stable voltage of 1.05 V in the initial operation. The applied electrolysis voltage slowly increased by 2.0%, from 1.05 to 1.07 V, after more than 50 h operations. The slight degradation in the electrolysis performance is not surprising as other reports have also noted this effect [22].

4. Conclusion

LSCM−Cu|LSGM|LSCF solid oxide electrolysis cells were firstly prepared and characterized with a gas mixture of 50% AH and 50% H_2 at different operating temperatures. The cells showed better electrochemical performance for steam and carbon dioxide co-electrolysis because of Cu impregnation, compared with LSCF|LSGM|LSCM solid oxide electrolysis cells without Cu impregnation due to the low electrical conductivity of LSCM. The cell resistance decreased with increasing the operation temperature and increased with increasing the CO_2 content at the same operated temperature. With the applied electrolysis voltage of 1.65 V and the operating temperature of 750 °C, the maximum consumed current density increased from 1.31 A cm^{-2} without CO_2 to 1.82 A cm^{-2} with 37.5% CO_2. The cell durability study for more than 50 h under co-electrolysis operation showed that Cu-impregnated LSCM is feasible as an effective cathode material for high temperature steam and carbon dioxide co-electrolysis.

References

[1] A. Hauch, S.D. Ebbesen, S.H. Jensen, M. Mogensen, J. Mater. Chem. 18 (2008) 2331–2340.
[2] K.R. Sridhar, C.S. Iacomini, J.E. Finn, J. Propul. Power 20 (2004) 892–901.
[3] K.R. Sridhar, B.T. Vaniman, Solid State Ionics 93 (1997) 321–328.
[4] S.D. Ebbesen, M. Mogensen, J. Power Sources 193 (2009) 349–358.
[5] F. Bidrawn, G. Kim, G. Corre, J.T.S. Irvine, J.M. Vohs, R.J. Gorte, Electrochem. Solid-State Lett. 11 (2008) B167–B170.
[6] C. Stoots, J. O'Brien, J. Hartvigsen, Int. J. Hydrogen Energy 34 (2009) 4208–4215.
[7] C. Li, Y. Shi, N. Cai, J. Power Sources 225 (2013) 1–8.
[8] T. Iwata, J. Electrochem. Soc. 143 (1996) 1521–1525.
[9] J. Sehested, Catal. Today 111 (2006) 103–110.
[10] R.M. Xing, Y.R. Wang, S.H. Liu, C. Jin, J. Power Sources 208 (2012) 276–281.
[11] C. Jin, C.H. Yang, F.L. Chen, J. Electrochem. Soc. 158 (2011) B1217–B1223.
[12] X.L. Yue, J.T.S. Irvine, Solid State Ionics 225 (2012) 131–135.
[13] C. Jin, C.H. Yang, F. Zhao, D.A. Cui, F.L. Chen, Int. J. Hydrogen Energy 36 (2011) 3340–3346.
[14] J. Wan, J.H. Zhu, J.B. Googenough, Solid State Ionics 177 (2006) 1211–1217.
[15] S. Tao, J.T.S. Irvine, J. Electrochem. Soc. 151 (2004) A252–A258.
[16] X.C. Lu, J.H. Zhu, Solid State Ionics 178 (2007) 1467–1475.
[17] Z.B. Yang, C. Jin, C.H. Yang, M.F. Han, F.L. Chen, Int. J. Hydrogen Energy 36 (2011) 11572–11577.
[18] Z.L. Zhan, W. Kobsiriphat, J.R. Wilson, M. Pillai, S.A. Barnett, Energy Fuels 23 (2009) 3089–3096.
[19] C. Graves, S.D. Ebbesen, M. Mogensen, K.S. Lackner, Renew. Sustain Energy Rev. 15 (2011) 1–23.
[20] Z.L. Zhan, L. Zhao, J. Power Sources 195 (2010) 7250–7254.
[21] X.D. Yang, J.T.S. Irvine, J. Mater. Chem. 18 (2008) 2349–2354.
[22] A. Hauch, S.H. Jensen, J.B. Bilde-Sorensen, M. Mogensen, J. Electrochem. Soc. 154 (2007) A619–A626.